International Conference
ENGINEERING MECHANICS 2010
Svratka, Czech Republic, May 10 – 13, 2010

PROCESSING FLOW VISUALISATION RECORDS BY CORRELATION COEFFICIENT EVALUATION IN SUB-IMAGES

V. Tesař*, V. Němička*

Summary: *Authors introduced a new method of processing flow visualisation images, aiming at identification of instability structures. In principle, the method utilises the structures' coherence. In two digital images, recorded at slightly different instants of time, the pixel pairs from the same position in the images are interrogated one by one. In each, vectors of the recorded quantity values are formed from n x n pixels in immediate neighbourhood. The correlation coefficient is then computed for the vector pair. High positive values of the coefficient indicate absence of change whereas values near zero indicate chaotic changes. Of interest are negative values, which indicate a coherent motion.*

1. Introduction

In many turbulent fluid flows, coherent structures are generated due to inherent hydrodynamic instability. Sometimes the structures may even have decisive influence on the processes taking place in the flow: e.g., in non-isothermal impinging jets the heat transfer is strongly dependent on the presence and character of the vortical motions developing from the instabilities. In some cases, such as in seeded jets at intermediate Reynolds numbers, the structures are well recognisable directly, by visual observation. Usually, a sophisticated image processing is necessary to identify them.

Apart from the relatively minor problem of the structure moving with the flow, away from a particular field of investigation — the main difficulty in experimental investigations of the vortical structures is their irregularity. There are two sources of the irregular behaviour:

a) stochastic character of turbulence which is superimposed - and into which the structures gradually decay, and
b) non-deterministic variations in the timing of structure formation.

The basic problem in experimental investigations of the structures is the "***degree of freedom gap***". The complex-shaped, convoluted and fast varying 3D objects are to be reconstructed from data acquired as 1D or 2D arrays. Classical measurements made point-wise by probes traversed to acquire a 1D data array are nowadays mostly supplanted by collecting the data optically in 2D – almost always in a plane, typically defined by a laser light sheet. Either simple visualisation or more sophisticated PIV methods (generating, in addition, also velocity information) are applied at a particular instant of time. Were the investigated 3D objects steady, reconstruction from 2D data might be done by tomographic methods (Kak and Slaney 2001) – repeating the 2D data collection at different plenes. However, reconstruction of fast

* Prof. Ing. Václav Tesař, CSc., RNDr. Václav Němička CSc. Ústav termomechaniky Akademie věd České republiky v.v.i.; Dolejškova 5, 182 00 Praha 8; tel.: +420 2 6605 2270, e-mail: tesar@it.cas.cz

changing 3D instability structures from 2D information – even if shifted sequentially either in time or in the direction of the third co-ordinate to cover 3D space, still presents a considerable challenge because both shifts cannot be made simultaneously (cf. Hesselink, Helman and Ning 1992). As a result, in the very principle such 3D reconstructions cannot be perfect.

2. Processing visualisation images

Identifying coherent motions in experimental data sets is done by processing the 2D data sets. Currently the most popular approach is decomposition of the flowfield into a "spectrum" of superimposed components of increasing spatial complexity. It is expected that the essential features of the flow are revealed by the principal first-order component (or at least a few components of the lowest order). A typical representative of this approach is SVD, *singular value decomposition*, with its two special cases, BOD and POD. The former (*bi-orthogonal decomposition,* also known as the method of empirical orthogonal functions) is practically suitable for reconstructing spatial features of laminar flows, because of the requirement of the data correlated in time. The latter – *proper orthogonal decomposition* (Bui-Thanh, Damodaran, and Willcox, 2004), also known (in other contexts, mainly in comparing two time series with some chaotic component) as Karhunen–Loéve expansion, Hotelling transform, principal component analysis, or method of empirical eigenfunctions. Though invented as long ago as 1901, only much later, in 1967, Lumley proposed POD as a tool for identification of dominant eddies in turbulence (Holmes et al. 1997, Chatterjee 2000). It is known in several alternatives and acquired recently considerable popularity because the software for its use is nowadays commercially available. It has been applied by a number of researchers to wide range of fluid flows — with varying degrees of success. Common failure often encountered is the energy content (evaluated from the velocity data) of the principal component not being significantly larger than that of higher-order eddies. This makes questionable the assumption of dominance of the low-order features. Also questionable are other fundamental assumptions on which the decomposition methods are based — e.g., the assumption of linearity which is basic for the idea of superpositions, the Gaussian character, the assumed importance of large variances, or the very basic feature of the orthogonality. From the point of view of detecting the instability structures, it may be questionable whether they are incorporated into the lowest-order components of the "spectrum". The limitation of SVD variants for the present purpose of evaluation of flow visualisation images is – besides the prohibitive cost of commercial packages - their current practical implementations oriented exclusively to analysing PIV data with velocity information.

3. Correlation coefficient

Present authors performed experimental investigations of typical flows containing the coherent structures (such as impinging jets – Tesař et al., 2008, Tesař and Němička 2009a, 2009b, Tesař, Němička, Šonský 2009), using flow visualisation in 2D light-sheet planes. The flows were seeded by micron-sized droplets — formed by water vapour condensation — into one of two mixed component flows. For detection and identification of the instability structures an original approach was used, which is the subject of the present paper. In proposing the new method, it was not attempted to supplant SVD or its POD variants, but mainly to offer an alternative having the advantage of not needing information about velocity and using only – much cheaper to obtain - flow visualisation data. Even more importantly, the method, being based on a wholly different idea, produces results of different character that may bring into forefront an information not immediately accessible in what is produced by the current commercial packages. Authors use their procedure in association with several variants of pic-

torial presentation of the results (such as alternative false colouring, posterisation or apodisation – and also evaluation of various averages). The present discussion, however, concentrates only on the central idea of extracting the coherent features present in the flowfield.

In principle, the detection of the structures in the new method is based on evaluating correlation between images obtained at different temporal phases of the vortex formation period – either between a pair of images recorded at a different instant of time or between an image and an average of images acquired in the same phase of a periodic process. The instability structures are identified due to their higher degree of coherence compared with the surrounding turbulence. If desired, by adjusting the scale of the detection, it is also possible to identify the turbulent eddies as long as they retain, foe a certain interval of time, their distinct character.

The basis of the method is computation of the correlation coefficient R between two vectors, $\mathbf{A}$ and $\mathbf{B}$, defined as

$$R = \frac{\mathbf{A}\,\mathbf{B}}{|\mathbf{A}||\mathbf{B}|} \qquad ...(1)$$

(where the product $\mathbf{A}\,\mathbf{B}$, in the numerator is the scalar vector product). The elements of the vectors, $\mathbf{A}$ and $\mathbf{B}$ are data values recorded from the pair of correlated images. The idea of evaluating the correlation coefficient, as a measure of relationship between two multi-valued variables, was developed by Pearson (1986) from a similar but slightly different idea introduced by F. Galton in the 1880s. In practical realisations, computation of eq. (1) is done using some of the procedures available in many programming language procedure libraries.

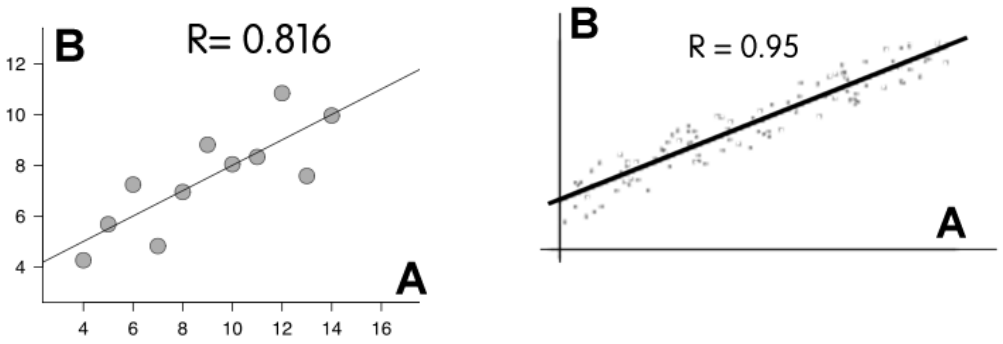

Figure 1 Two examples of the correlation coefficient R between two data vectors x and y, interpreted as the measure of the scatter in their linear dependence $\mathbf{B} = f(\mathbf{A})$.

The most apparent way how to present a dependence $\mathbf{B} = f(\mathbf{A})$ between two multi-valued variables is, of course, to plot the Cartesian diagram - as it is done in the two examples presented in Fig. 1. The value of the correlation coefficient is a measure of the scatter of the linear dependence between the two data vectors: the higher is the value R the better is the fit by the straight trend line – as demonstrated in the top part of Fig. 2. Note that the magnitude of the correlation coefficient is dependent neither on the slope or on the intercept values nor is it influenced by any non-linear relation between the two data sets. The latter means, in other words, that even if the dependence in a diagram like those presented in Fig. 1 were following quite smoothly a curve, e.g., a quadratic one, the computation of the correlation coefficient remains based on fitting a linear trend line through such data points – so that all the deviations from the linearity, however regular, are treated as if they were a chaotic scatter.

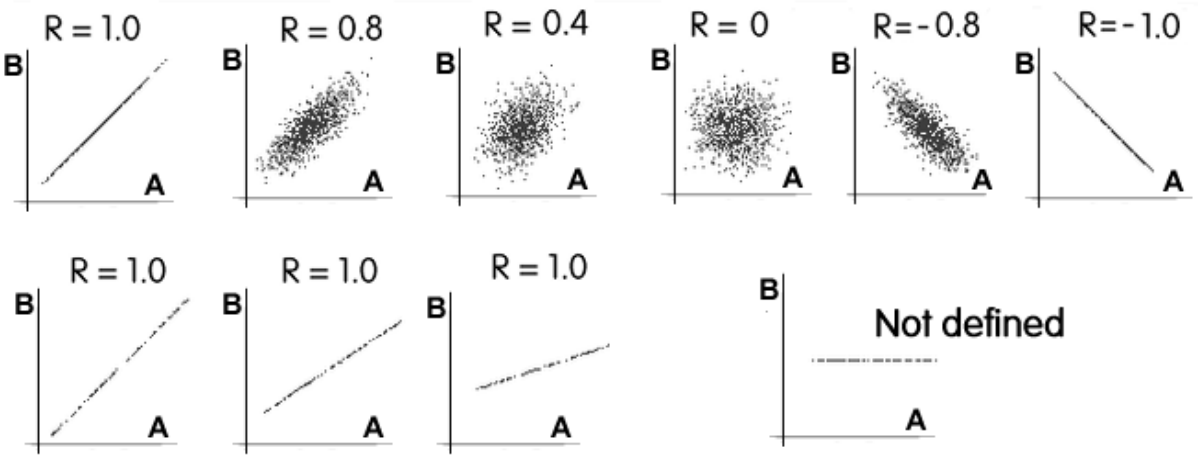

Figure 2 Some other examples of the correlation coefficient values for various linear dependences presented as the Cartesian diagrams $\mathbf{B} = f(\mathbf{A})$. Note that R does not depend on the slope of the linear relationship (the same R=1 applies to the whole bottom row of cases with different slope) – but changes sign if the slope is negative.

Note the absence of the result (failure of eq. (1)) in the case of the independence shown in Fig. 2 - with zero variation of one of the two variables. R cannot be evaluated as this would involve division by zero in eq. (1). To avoid an inconvenient stopping of the computation, it is usual to substitute $R = 0$ for the result in such cases. In some (rather exceptional) situations when applying eq. (1) to the processing of images, this may generate regions of zero R values that have no physical meaning and have to be interpreted taking this exceptional situation in mind.

There are other alternative interpretations of the meaning of the correlation coefficient R that may provide a useful mental image to follow. Particularly useful may be the idea of R characterising the angle between the two vectors $\mathbf{A}$ and $\mathbf{B}$. This is based on the geometric interpretation of the scalar product $\mathbf{A}\mathbf{B}$, Fig. 3. The two vectors are parallel if $R = 1$, mutually perpendicular if $R = 0$, and lead into the opposite directions for $R = -1$. The instructiveness of this geometric interpretation is, of course, lost for the higher-dimensional vectors.

Of particular interest for the use of eq. (1) in processing two images recorded one after another is yet another interpretation — the one based on the idea of replacement of a particular element value in the vector $\mathbf{A}$ by the value at the same position in the vector $\mathbf{B}$. The values may be the intensities on the greyscale: for $R = 1$, the values are equal, black colour in $\mathbf{A}$ is followed by the same black colour in $\mathbf{B}$. For $R < 1$ the replacement colour is not black but a shade of grey - and for $R = -1$ the black colour is replaced by its opposite, white.

In the use for comparinson of two images, the data values of the investigated variable (which in this case is usually the local light intensity values stored at the particular pixel positions) are stored as matrices. The correlated vectors, $\mathbf{A}$ and $\mathbf{B}$, are constructed from the matrices by placing all the rows of the matrix one after another into a single long vector. If the images are identical, then the correlation coefficient is simply

$$R = 1 \qquad \ldots (2)$$

and this fact is of practical importance for comparison of a pair of images as to their disparity.

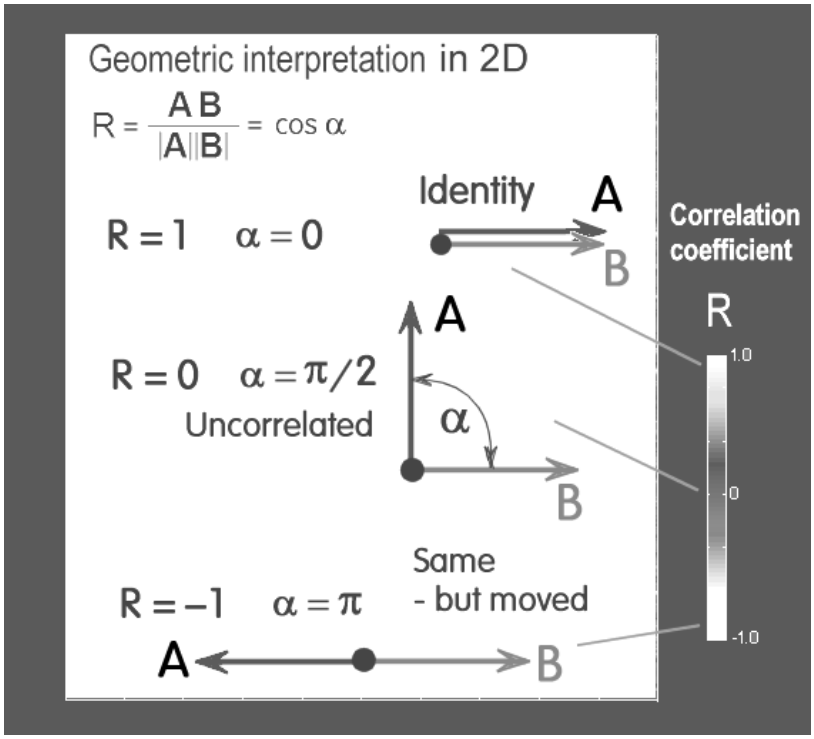

Figure 3 Another interpretation of the meaning of the correlation coefficient – applicable to the simplest case of two-element vectors **A** and **B** (i.e. both of dimension 2). In this case the expression eq. (1) represents the angle α between the two vectors.

This has been already a standard processing method of images recorded by security surveillance cameras. Watching the camera images in which nothing new happens is extremely boring task for security personnel. Computation of eq. (1) and generating an alarm if $R < 1$ is nowadays a common procedure. A similar detection of $R < 1$ has found use in other security applications such as tamper detection and tagging (tamper-proof fingerprinting of objects).

What is required in these cases is just an indication of identity. The tremendous loss of information – obtaining, by use of eq.(1), just a single number from all the data contained in image pixels – is in these applications an advantage. Similar uses were developed in medicine (monitoring of changes such as, e.g., detection of growth of tumors to indicate their malignity). Analogous use in biology is described in Sviridov et al., 2006. Theoretically, the detection of a change having occurred by the fulfilment of eq. (2) is not absolutely safe. The condition may be fulfilled also if the change in the surveyed image is precisely compensated for by an opposite change in other pixels. This, however, in most security applications is merely a theoretical possibility (and, at any rate, is left to the judgment of the personnel that is to be present anyway).

Because of the linearity implied in the definition of the correlation coefficient, such compensation, however, takes place also whenever an object in the image undergoes a linear transformation: rotation, translation or (within some practical limits dictated by the pixel size) dilatation. The linear transformation does not change the value of the evaluated coefficient R. This may have useful practical consequences, such as, e.g., insensitivity to a not exactly the same camera position in the tumor monitoring mentioned above.

4. Authors' new sub-image method

The computation of the single value of the correlation coefficient evaluated in the known approach to comparison of images discussed above, of course, means a huge loss of information and cannot provide any useful information about the changes that took place in the cases characterised by $R < 1$.

The basic idea of the new authors' method is evaluation of the local correlation coefficients in sub-images sequentially constructed for all corresponding pixel pairs in the same position in the image pair. All the pixels in the image are interrogated one by one and the construction of the comparison vectors $\mathbf{A}$ and $\mathbf{B}$ is repeated in each of them. At each location thus the local character of the change that took place between the recording of the two images is evaluated. It is computed as the local value of the correlation coefficient – and usually plotted using some form of false colour rendering. The value makes it possible to identify the character of the change that took place during the interval. A suitable presentation by an apparent (false) colour focuses attention on this position in the image. In particular, it is possible to discriminate between the features that did not change (and are therefore, as a rule, uninteresting) and the features associated with the coherence of the structures. These become usually immediately apparent and this way the method suppresses the influence of the chaotic character of the turbulence however much it covers the investigated structures.

There is a choice as to which images are used in the correlated pair. Interesting results were, e.g., obtained by correlating an instantaneous image with the image obtained by phase

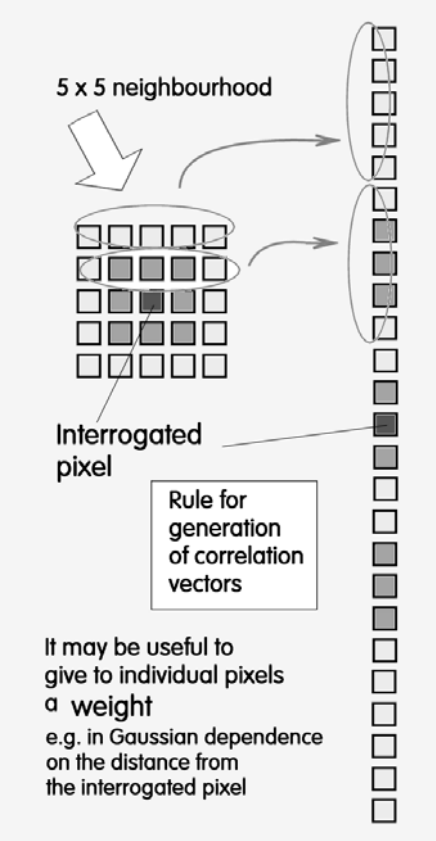

Figure 4 One of the methods of construction of the vectors $\mathbf{A}$ and $\mathbf{B}$ (here of dimension 25, which is most often used by the authors in practical tasks) for the computation of the local values of the correlation coefficient. The vectors are set up from the 5x5 sub-image in the neighbourhood of the particular interrogated pixel.

averaging over several periods of a periodic or quasi-periodic process (many instability structures are quasi-periodic). Most correlation computations so far, however, were made using image pair recorded in succession, after a short time interval. The recorded changes are then, of course, rather small and it is a positive feature of the correlation technique that it enhances mostly the features at a local scale – as it takes into the correlated vectors **A** and **B** just the pixels from the immediate neighbourhood of the interrogated pixel – Fig. 4.

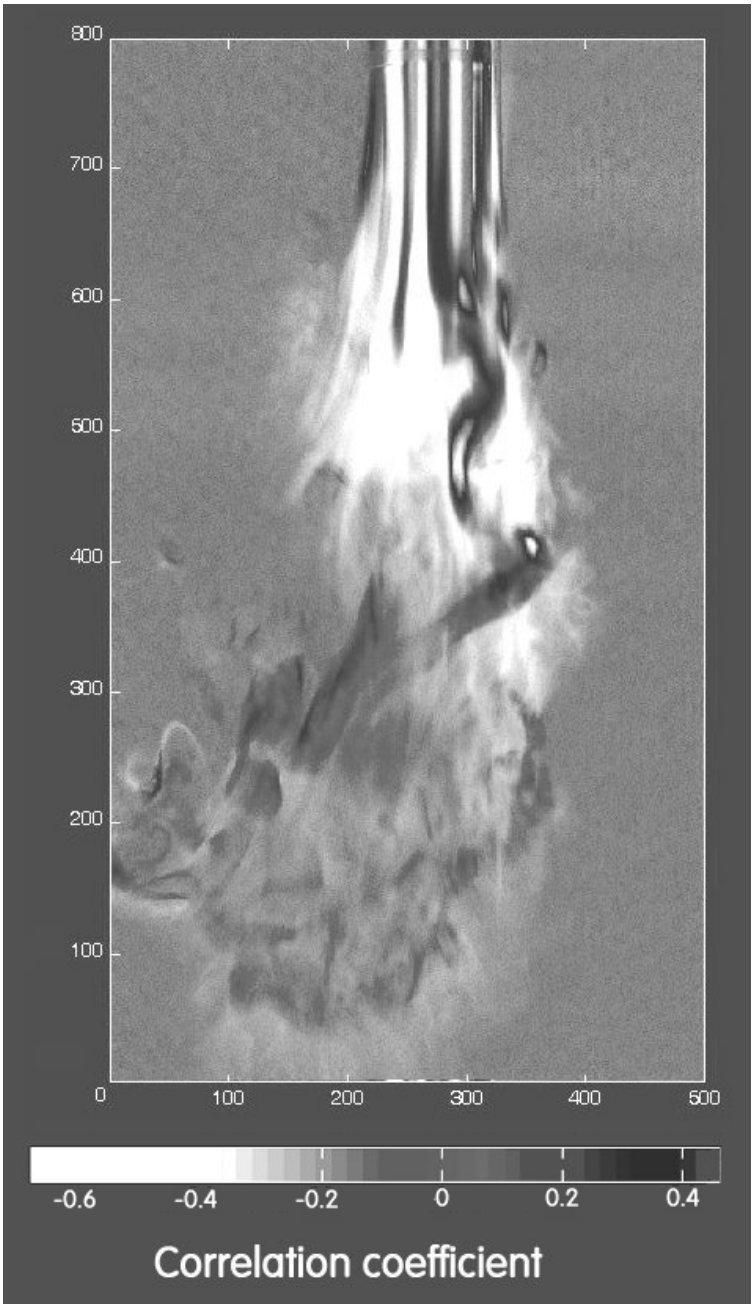

Figure 5 Example demonstrating practical importance of the sub-image method in fluid mechanics: an example of computed distribution of the correlation coefficient in a jet flow (oriented vertically downwards, visualised by addition of water). The region with negative values of the coefficient (white in this picture) represents the investigated instability structure. Noteworthy is the change in the jet flow flow dynamics: the laminar flow near the nozzle (above) passes through the instability (white) and undergoes there a fast transition into turbulence (below).

There is also a wide choice as to which neighbouring pixels are chosen and in what manner they are arranged in the correlated vectors **A** and **B**. The most often used procedure (taking the sub-matrix rows and placing them one by one) shown in Fig. 4 is just one of many available possibilities. The size n of the n x n sub-images, of course, is reflected in the size of the structures that this method is capable of detecting. As mentioned in Fig. 4, it may be useful to suppress the influence of the pixels from more distant neighbourhood by giving less weight to the values to them. It is also, for example, possible to emphasise one direction (vertical, horizontal, or at some inclination) of the detected features in the images by choosing for the construction of the vectors **A** and **B** the pixels in rows, columns, or some pixels in skewed arrays.

As an example of an identified coherent region in a pair of images of a submerged air jet, Fig. 5 presents the grey-scale coded distribution of the computed distribution of the local correlation coefficients. The insight into the dynamics of the changes in such a jet acquired by the discussed approach is obvious.

5. Characteristic features of the method

It is useful to present at this stage some examples of the functioning of the sub-image correlation method - so as to show its advantages as well as weaknesses. First, let us investigate how it handles one of the main problems in processing flow visualisation images of cases of practical engineering importance, the ubiquitous turbulence. It produces a various degree of chaos leading to decreased correlation between the pictures. The discussed method can bring quantification of the degree, giving a numerical value of the magnitude of the present chaos. As an instructive example, the following Figs. 6 to 11 demonstrate the influence of the presence of the chaos on a simple example of a picture of a simple object – a cylindrical body, shown in Fig. 6. With the superimposed Gaussian chaos the same object is shown in the following Fig. 8. Performing a processing of this image pair (Figs. 6 and) by the standard pro-

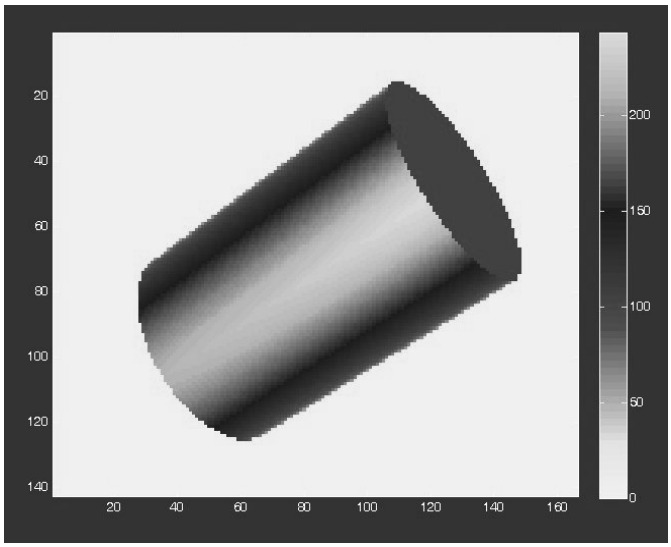

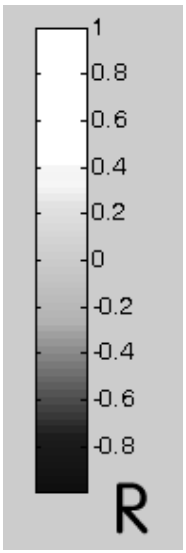

Figure 6 (Left) An example of an image of a simple object (a cylinder chosen to be similar to a rotating vortex).
Figure 7 (Right) The greyscale colourbar used for presentation of distributions of evaluated correlation coefficients R.

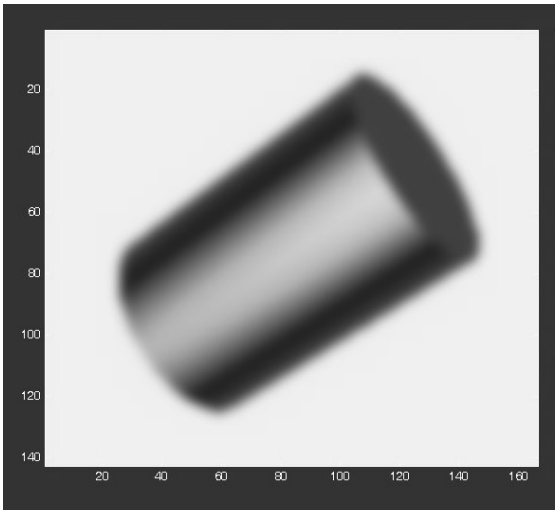

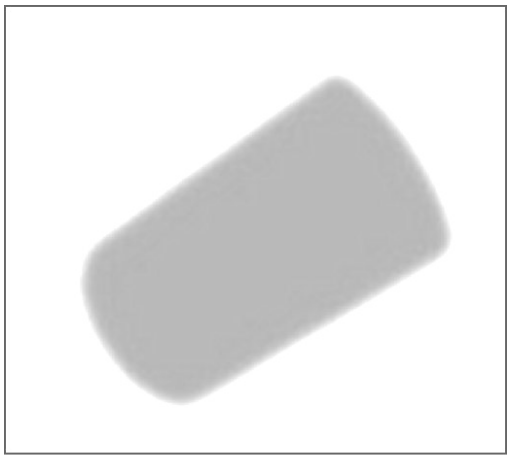

Figure 8 (Left) An image of the same object as in Fig. 6 complicated by superimposed Gaussian chaos.

Figure 9 (Right) Computed distribution of the coefficient of correlation R between the images in Figs. 6 and 8. Due to the presence of the (homogeneous) chaos, the correlation coefficient values are lower than white colour identity $R = 1$ (as it is shown at the top of the scale in Fig. 7) – it is here grey indicating the chaos (which is near to $R = 0$, but here the chaos is not very strong and the values are positive).

cedure – using the 5×5 local neighbourhood values in the correlated vectors according to Fig. 4 – produced the distribution of the correlation coefficient values as presented in Fig. 9. Obviously, despite the identity of the objects, the chaos decreases the coefficient to $R < 1$. Since this is an artificial chaos of constant intensity, the value R is identical over the region in which the two image objects coincide, decreasing on the circumference of the region. The value reaches $R = 1$ (the white colour in the colourbar, Fig. 7) in the outer parts of the images, where there is no change.

As it might be expected, a similar comparison of two images Figs. 6 and 10, with larger difference between them caused by the presence of chaos, leads to the similar distribution of the correlation coefficient in the image plane, Fig. 11. The region of the values $R < 1$ is now darker, indicating less mutual correspondence, and also the blurred character of the boundaries is more pronounced. In real visualisation images of turbulent flows, of course, the chaos is present in both images of the compared pair. The correlation coefficient in that case is not $R = 1$ in spite of perhaps similar visual impression, just because the chaos is stochastic and the turbulence does not remain the same after the interval of time elapsed between the recording of the two images.

Let us now focus the attention on the character of the representation, in the plane of the local correlation coefficient values, of the effect of a motion of the object. Two images recorded with some time interval between them, will differ in the position of the object. If the object moves coherently, as if it were a solid body, the change during the interval between recordings is identified as a negative value $R < 0$. In the case of the object having sharp edges and coloured black on white background, the motion will result in one extreme ("black") colour of the inside of the body replaced by the opposite extreme (" white") colour of the background. This change into the very opposite (opposite directions of the two vectors,

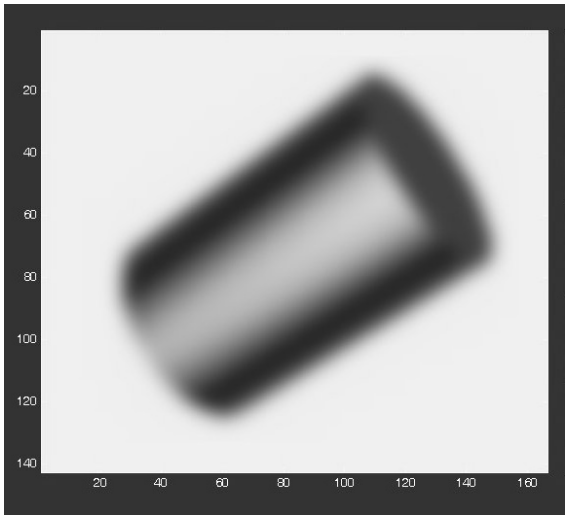

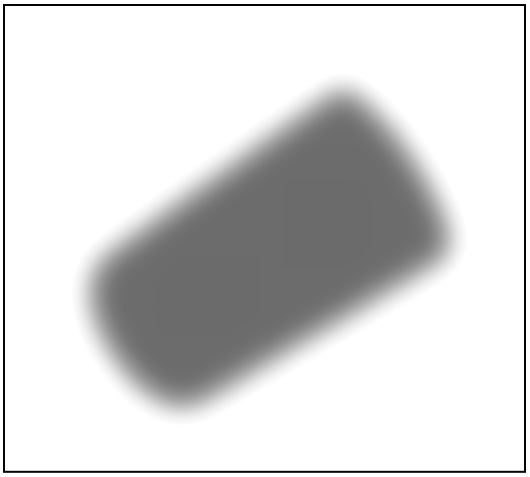

Figure 10 (Left) An image of the same (cylindrical) object as in Fig. 6, presented here with increased intensity of the chaotic component.

Figure 11 (Right) Computed distribution of the coefficient of correlation R between the two images in Figs. 6 and 10. Comparison with the previous Fig. 9 shows that the increased level of chaos has led to lower R values, quite near to R = 0 (note the darker grey shade - Fig. 7). Also, the chaos has led to significant blurring of contours of the dark region.

cf. Fig. 3) is in an agreement with the result R = -1 on that part of the image plane from which a narrow strip of the body circumference was removed.

In its details, however, the character of the correlation coefficient distribution may become quite complex, because of the inevitable passage through the R values starting at R = 1 in the background part that did not experience the change. It is again useful to follow the character of the correlation coefficient representation in some drastically simplified case of an artificially constructed object.

A suitable model object is presented in Fig. 12. Shown there is the dependence of the light intensity value (vertical co-ordinate in Fig. 12) on the horizontal distance in the image plane. In the next Fig. 13, the object is shown in the two images at different instants of time.

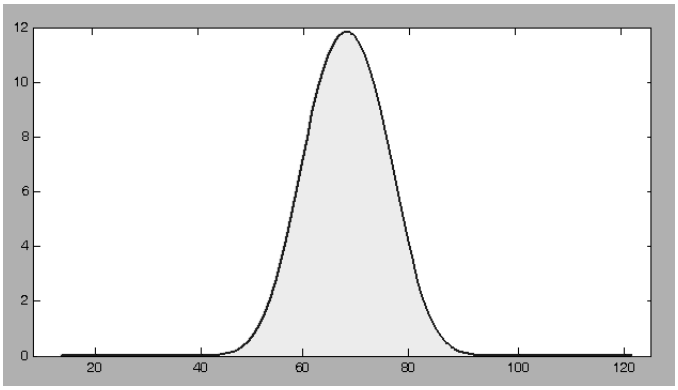

Figure 12 Model object used for investigation of the properties of the discussed image processing method: a Gaussian “hill” having no clearly defined boundaries. Here it is shown in section by a vertical plane passing through the “summit”.

The vertical co-ordinate from Fig. 12 is presented in the two images in Fig. 13 by means of the false colouring. This uses the transformation function represented by the colourbar at the extreme right-hand side in Fig. 13. The shape of a " hill" - actually a distribution described by the Gauss function – was chosen to approximate the generic regions with not very clearly defined boundaries. Here, of course, the shape decreasing in the radial direction is defined by a deterministic function whereas real flowfield objects have the boundaries poorly defined due to the presence of chaos, which absent is in this simple example.

Since the object in this case has moved as a whole (it moved, in fact as a solid body, upwards by 7 pixels – a distance commensurable with the size of the neighbourhood chosen

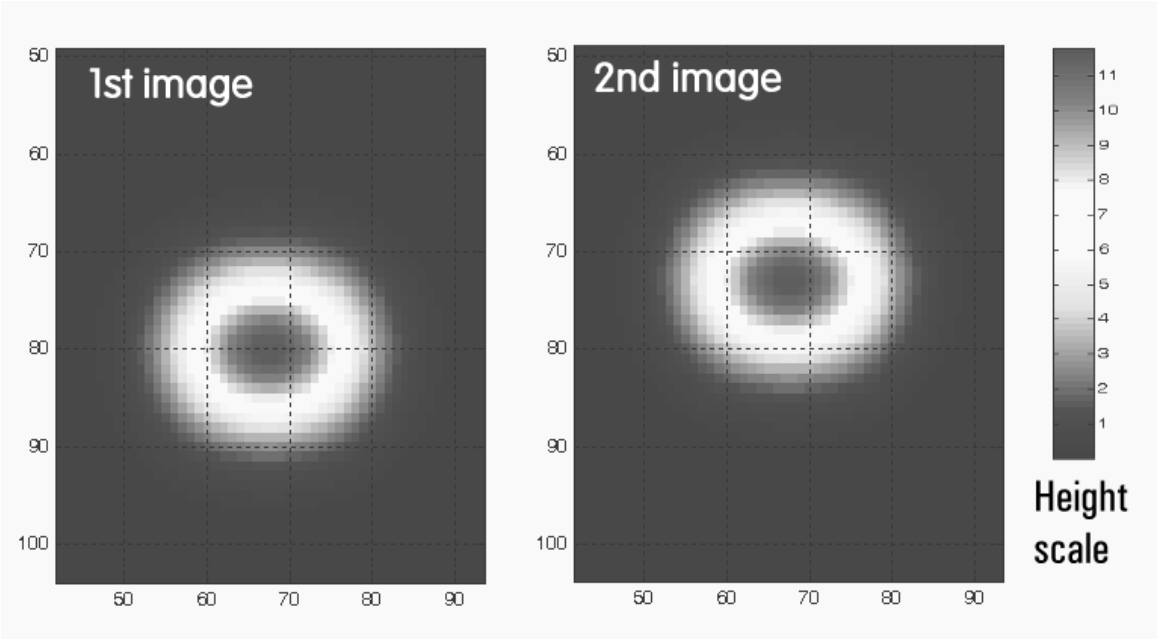

Figure 13 Two images of the model object from Fig. 12. Between the time these images were recorded, the object has moved upwards by 7 pixels. The vertical co-ordinate in Fig. 12 is here represented by the false grey colouring according to the scale shown at right.

in construction of the two compared local vectors **A** and **B** as shown in Fig. 4) the computed values of the local correlation coefficient R indeed do reach the negative values $R < 0$. This is presented in Fig. 14. It should be noted that the false colour function used (and defined in Fig. 14 by the colourbar at the extreme right-hand side) is a different one than the case of Fig. 7 used in the previous examples. This colouring, with both ends of the colourbar dark, resulted from conversion into greyscale of the original full-colour definition.

The example of the "hill" shaped object is, of course, artificial. It is useful for study of the details of the correlation procedure, but too far removed from actual situations usually encountered in flowfield studies. It is useful to continue the study of the local correlation coefficient representations by yet another case, with the object geometry somewhat more akin to real situations. It is actually again the case of the cylindrical model body as presented above in Fig. 10, but its images (Figs. 17 and 18) now to not show the external appearance of the body, but in accordance with the actual situation in which the structures are identified in laser-light sheet sections, what is presented in Figs. 17 and 18 are just planar regions produced by plane cut passing through the cylinder. To provide a more realistic setting, the perimeter of

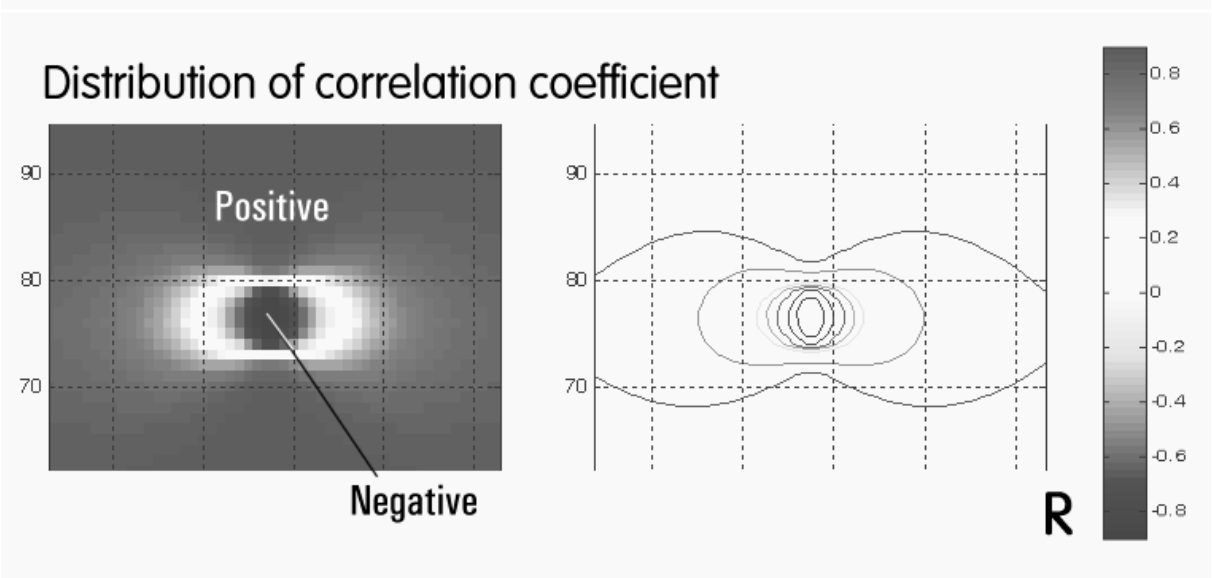

Figure 14 Demonstration how the correlation coefficient of the two images attains a negative value if the object moves during the interval between the recordings of the two images. The correlation coefficient R is here computed for the two images from Fig. 13 by the discussed sub-image evaluation method. The positive value R = 1 far from the objects shows absence of any local change there.

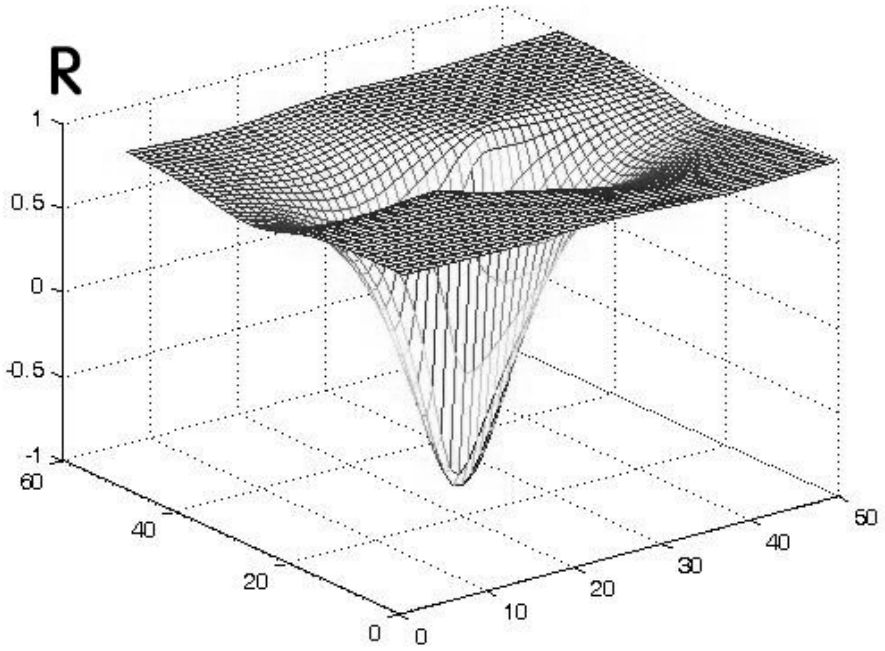

Figure 15 3D view of the distribution of the correlation coefficient R presented in Fig. 14, evaluated by application of the developed image-processing procedure on the simple test object from Figs 12 and 13. The procedure actually leads to distribution with somewhat complicated details. The value R = -1 is reached in a single point.

the region is blurred by simulated chaos of turbulence – in fact this is a homogeneous Gaussian "chaos" computed as a superposition of a deterministic formula. The cylindrical body now moves in the direction of the cylinder axis. While in Fig. 17 the region is roughly centred, positioned in the middle of the image, the second Fig. 18 is recorded after a short time

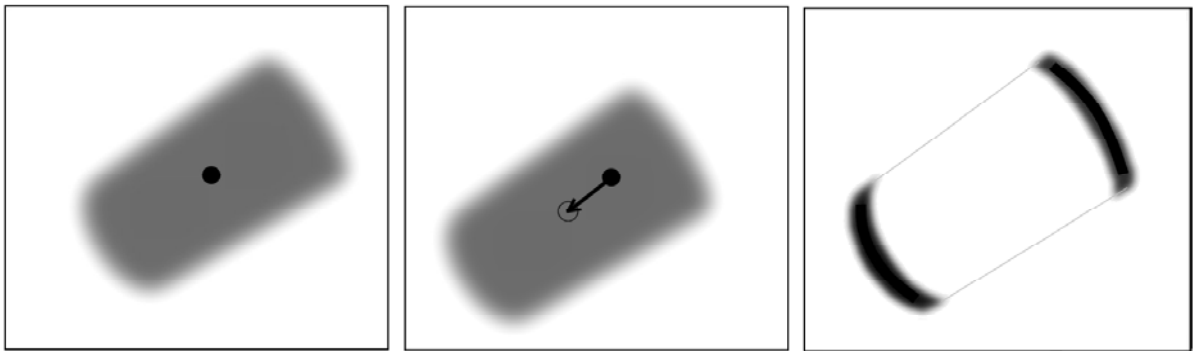

How the discussed method identifies motion of an object in the image plane – shown on a simple model case:

Figure 17 (Left) Initial position of the region. It is a result of laser-light sheet intersecting the cylindrical test object from Fig. 10, with superimposed gaussian chaotic motion.

Figure 18 (Centre) Position of the region from Fig. 17 in the second image. The mody moves in the direction of the cylinder axis.

Figure 19 (Right) Computed distribution of the coefficient of correlation R between the images from Fig. 17 and Fig. 18. Because the object has moved as a solid body, negative values near to R = -1 are found at the ends of the region produced by the light section.

interval. The region has in the meantime moved. The motion is indicated by the black dot drawn in Fig. 17 in the middle of the dark region. The dot is again drawn in Fig. 18, where it is immediately seen to be away from the centre of the dark region – which is marked by an empty circle. The distance travelled by the region is marked by the arrow. Because the dark region has moved as a solid object, not changing its shape, the method of local correlation coefficients in sub-images produces values R = -1 in the areas in which the dark regions in the two images doe not coincide. For the presentation of the coefficient values, the greyscale colourbar used for presentation the results with the cylindrical object in Fig. 7 applies again. The presentation in Fig. 19 shows the fully black regions in the areas of non-coincidence. In the example of a simple, artificially designed object presented in Figs. 17 to 19 the motion

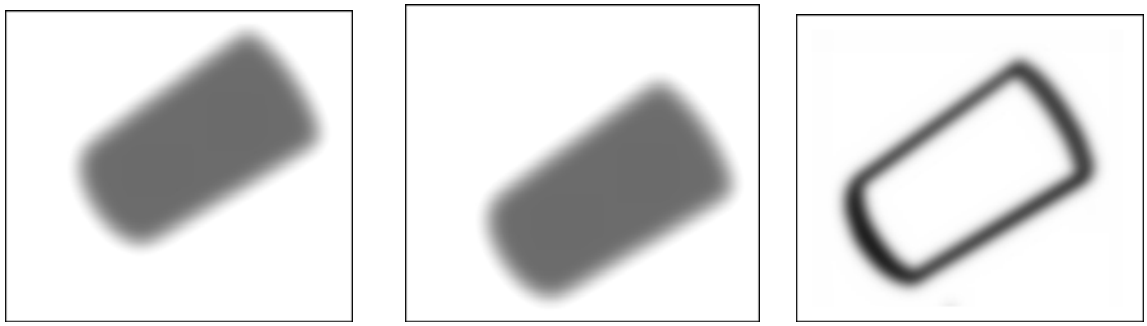

A more general example of detection of correlated motion of an object in a plane:

Figure 20 (Left) Initial position of the object – the grey region (with superimposed chaos).

Figure 21 (Centre) Position of the object in the second image. The body has moved in a more general way – not only axially as was the case in Fugs. 17 and 18.

Figure 22 (Right) Resultant computed distribution of the local coefficients of correlation R. obtained for the two compared images Figs. 20 and 21.

to be detected was somewhat special – in the axial direction. A more general case is presented in the otherwise similar next example presented in Figs 20 to 22. The computation of the coefficient R in the final result Fig. 22 has produced a contour of the moving object (the section through the cylinder from Fig. 10). This is a very general result, observed already earlier in processing images of jets and impinging jets – Tesař et al., 2008, Tesař and Němička 2009a, 2009b, Tesař, Němička, Šonský 2009, where the detected vorticed were clearly marked by values R = -1 in their cicumferences.

It is obvious that what the discussed method identifies of the detected objects is producing **contours** of the moving objects in the plane of correlation coefficients R. This property – revealing contours of coherent objects – us the basic property of the method.

6. Question of tomographic imaging

The essential problem mentioned in the Introduction part of the present paper is the difficulty of reconstructing the 3D structures of interest from the arrays of 2D images. The

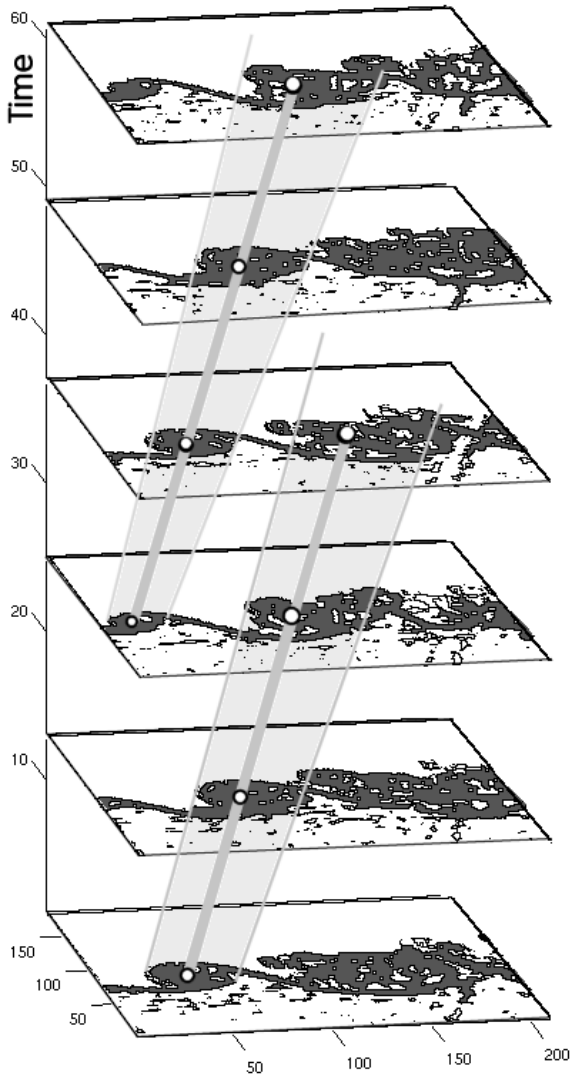

Figures 23 If the processed images are recorded at short intervals between them, the detection of the contours of structures in the flow moving coherently makes it relatively easy to reconstruct the structures as spatial objects. The identification of the contours is particularly helpful.

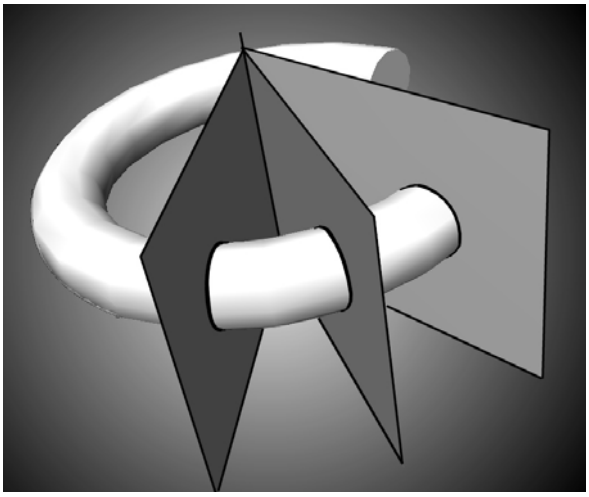

Figures 24 Schematic representation of reconstructing a helical vortical structure as a spatial object from the contours (heavy black curves) in the equal-phase planes.

images are planar and may be recorded in known spatial positions of the planes. For example, in the investigations of helical structures in jets and impinging jet flows – Tesař et al., 2008, Tesař and Němička 2009a, 2009b, Tesař, Němička, Šonský 2009 – the recording is controlled by phase trigger so that it is possible to investigate – one by one – the phase angle locations corresponding to the whole period of the triggered beginnings of structure generation. It is also possible – as shown in Fig. 23 – to record the individual stages of the progress and development of the vortical structures as they pass through the interrogation window.

The property of the structure detection method – the fact that the correlation procedure generates the contours of the light-sheet sections through the structures – makes it easily possible to use these sections as inputs into the tomographic processing. The image planes are first arranged into their proper spatial positions and then, in the second step, the contours found in individual planes are mutually connected by smooth surfaces to set up the spatial three-dimensional bodies.

7. Conclusions

In this paper, new technique is introduced for detecting and investigation of structures present in fluid flows due to hydrodynamic instabilities. The fundamental problem is how to extract information about unsteady three-dimensional objects from two-dimensional flow visualisation images. The other problem is the structures are submerged in chaotic turbulence. Because of the unsteady character of the objects of interest, turbulence cannot be simply filtered out by statistical averaging. Authors describe a recently introduced method of processing flow visualisation images, different from the know POD approach. In principle, the method operates with two digital images, recorded at slightly different instants of time. All pixels of this pair are processed one by one by computations of the correlation coefficient R between the vectors constructed from the values in the neighbouring pixels – mostly in the pair of n x n pixel sub-images placed one by one. The results is a map of the correlation coefficient values. In places where the coefficient values are positive and high (near or equal to R = 1 the flowfield does not exhibit any changes. Values near to R = 0 indicate chaotic behaviour. Of main interest are negative values, which indicate a coherent motion. The regions of R < 0 are usually found on the contours of the instability structure regions.

8. Acknowledgements

The authors acknowledge gratefully the support by the grant IAA200760705 from the Grant Agency of the Academy of Sciences of the Czech Republic, and by the grant 101/07/1499 from the Grant Agency of the Czech Republic. In their experiments, the authors were dependent on help of Dr. J. Šonský, Miss R. Kellnerová, and Mr. L. Kukačka.

References

Bui-Thanh T., Damodaran M., Willcox K. (2004) Aerodynamic Data Reconstruction and Inverse Design Using Proper Orthogonal Decomposition, *AIAA Journal*, Vol. 42, No. 8

Chatterjee A. (2000) An Introduction to the Proper Orthogonal Decomposition, *Current Science*, Vol. 78, p. 808

Delville J., Ukeiley L., Cordier L., Bonnet J.P., Glauser M. (1999) Examination of large-scale structures in a turbulent plane mixing layer. Part 1. Proper orthogonal decomposition, *Journal of Fluid Mechanics*, Vol. 391, p. 91

Hesseling, L., Helman J., Ning P. (1992) Quantitative Image Processing in Fluid Mechanics, *Experimental Thermal and Fluid Science*, vol. 5, no. 5, p. 605, 1992

Holmes P.J., Lumley J.L., Berkooz G., Mattingly J.C., Wittenberg R.W. (1997) Low-dimensional models of coherent structures in turbulence. *Physics Reports*, Vol. 287, p. 337

Kak A. C., Slaney M. (2001) *Principles of Computerized Tomographic Imaging,* Society of Industrial and Applied Mathematics, ISBN: 089871494X, New York

Pearson K. (1896) Mathematical contributions to the theory of evolution. III. Regression, heredity and panmixia" *Philos. Trans. Royal Soc. London Ser. A* , **187** p. 253

Regunath G., Tesar V.**,** Zimmerman W.B.J., Hewakandamby B.N., Russell N.V.(2006), Experimental Investigation and Visualization of Helical Structures in a Novel Swirling Jet, *Proc. of FEDSM06, ASME Joint U.S. – European Fluids Engineering Summer Meeting*, Technical 32-5 Optical Methods 2, Miami, FL, July 2006

Sviridov A.P., Ulissi Z., Chernomordik V., Hassan M., Gandjbakhche A.H. (2006) Visualization of Biological Texture Using Correlation Coefficien Images, *Journal of Biomedical Optics,*Vol. 11, p. 060504-1

Tesař V., Němička V., Šonský J., Kukačka L., Pavelka M. (2008) Effect of Azimuthal Excitation in the Nozzle Exit on Structures Formed in Submerged Jets, *Proc. of Colloquium FLUID DYNAMICS 2008*, ISBN 978-80-87012-14-7; publ. by Institute of Thermomechanics AS CR, v.v.i., Prague, October 2008

Tesař V., Němička V., Šonský J. (2009) Extracting Information About Coherence in Jet Flows, *Proc of Conf. "Engineering Mechanics 2009*", ISBN: 978-80-86246-35-2, May 2009

Tesař V., Němička V. (2009a) Study of Vortical Structures in Impinging Jets - New Methods and Approaches*, Proc. of ExHFT-7, the 7th World Conference on Experimental Heat Transfer,Fluid Mechanics and Thermodynamics,* Krakow, Poland, June-July 2009

Tesař V., Němička V. (2009b) Phase-Synchornised Investigations of Triggered Vortices in Impinging Jets, *Proc of Conf. "Engineering Mechanics 2009*", ISBN: 978-80-86246-35-2, May 2009

Tesař V, Zimmerman W.B.J., Regunath G. (2005), Helical Instability Structures in Swirling Jets, *Proc of the 8th International Symposium on Fluid Control, Measurements, and Visualization FLUCOME 2005*, Chengdu, China